ADVANCED FUNCTIONAL MATERIALS
www.afm-journal.de

A General Synthetic Strategy toward Highly Doped Pyridinic Nitrogen-Rich Carbons

Xiaoling Mou, Jiaxin Ma, Shuanghao Zheng, Xingkun Chen, Frank Krumeich, Roland Hauert, Ronghe Lin, Zhong-Shuai Wu,* and Yunjie Ding**

Doping carbon materials with p-block elements such as nitrogen is an effective approach to tune electronic properties of the framework and can endow the host's new characters. To date, highly doped carbons with tunable nitrogen speciation are still less explored due to the grand challenge in fabrication; for example, the typical synthesis based on the pyrolysis of nitrogen-containing precursors shows a trade-off between the total nitrogen content and the carbonization temperature, limiting the value to ≈12 wt% at 1073 K. Herein, intensifying ring opening of cross-linked polymers through controlled pre-oxidation followed by conventional pyrolysis is demonstrated as an elegant method to circumvent this challenge. In addition to fine tunability at different nitrogen speciation, this strategy can increase the nitrogen content by two- to threefold (maximum ≈22 wt%) and shows general viability in six different N-bearing (co)polymers. The highly doped pyridinic nitrogen-rich carbons show i) a remarkable capacity of 879 mAh g^{-1} at 0.1 A g^{-1} and excellent cycling performance in lithium ion batteries, and ii) significantly boosted catalytic performance in the selective oxidation of diverse substrates. Therefore, this facile synthetic strategy and the tunability at nitrogen functionalities will greatly broaden the applications of this new class of functional materials.

1. Introduction

Introducing foreign atoms into carbon framework is a general approach to tune the electronic and spin structure via the creation of vacancies or defects.[1–3] Among various dopants, nitrogen is most extensively studied, and thereby the N-doped carbon (NC) ensembles have shown promising prospects in numerous fields including CO_2 capture,[4–6] metal ion batteries,[7–9] electro-[10–12] and thermal-catalysis,[13–15] and so on. For these materials, the total nitrogen content and the bonding configurations in a given carbon matrix can be viewed as the two key factors that largely determine the properties and performance of the hybrids. Systematic control over these two characters would allow the establishment of structure-performance relationships and ultimately of design rules of more advanced materials for targeted applications. In this context, several distinct strategies have been proposed to enrich the specific type of nitrogen species, such as pyridinic[9,16–21] or quaternary nitrogen.[22,23] However, the total N concentrations, in such cases, are usually relatively low, plus the synthesis is always limited to a very specific approach. To the best of our knowledge, a generalized synthetic protocol affording simultaneously a high nitrogen content (up to 22 wt% in bulk) and delicate tuning of the nitrogen speciation has not been reported yet.

Carbonization of N-containing polymers is widely used as an effective approach to fabricate NCs.[24,25] Such derived materials, however, frequently show a decreased nitrogen content at elevated carbonization temperature. For instance, the polymers pyrolyzed at 1073 K possess around 12 wt% N that is much lower than those of the precursors.[26] In addition, as quaternary N is favored at high temperatures owing to the higher thermostability, the conventional treatment offers

---

Dr. X. Mou, Dr. X. Chen, Prof. R. Lin, Prof. Y. Ding
Hangzhou Institute of Advanced studies
Zhejiang Normal University
Gengwen Road 1108, Hangzhou 311231, China
E-mail: catalysis.lin@zjnu.edu.cn

J. Ma, Dr. S. Zheng, Prof. Z.-S. Wu, Prof. Y. Ding
State Key Laboratory of Catalysis
Dalian Institute of Chemical Physics
Chinese Academy of Sciences
Zhongshan Road 457, Dalian 116023, China
E-mail: wuzs@dicp.ac.cn; dyj@dicp.ac.cn

J. Ma
University of Chinese Academy of Sciences
Yuquan Road 19A, Shijingshan District, Beijing 100049, China

Dr. S. Zheng, Prof. Z-S. Wu, Prof. Y. Ding
Dalian National Laboratory for Clean Energy
Dalian Institute of Chemical Physics
Chinese Academy of Sciences
Zhongshan Road 457, Dalian 116023, China

Dr. F. Krumeich
Institute for Chemical and Bioengineering
Department of Chemistry and Applied Biosciences
ETH Zurich
Vladimir-Prelog-Weg 1, Zurich 8093, Switzerland

Dr. R. Hauert
Swiss Federal Laboratories for Materials Science and Technology
EMPA
Überlandstrasse 129, Dübendorf 8600, Switzerland

The ORCID identification number(s) for the author(s) of this article can be found under https://doi.org/10.1002/adfm.202006076.

DOI: 10.1002/adfm.202006076

limited control of the different nitrogen functionalities, particularly for highly doped carbons. Since all the nitrogen functionalities of NCs are evolved from the analogs of the polymer precursors, tuning the relative nitrogen speciation of the polymers before pyrolysis might impose alteration of nitrogen functionalities in the descendant. Earlier studies showed that heating polyaniline (PAni) at low temperatures (≤473 K) in air or in vacuum leads to cross-linking of the polymer mainly through the formation of the Ph-NH-Ph structure (Ph = phenazine ring).[27] This ensemble was suggested as the precursor of the pyrrolic and quaternary nitrogen (N5 and N3) on the basis of detailed ^{15}N NMR experiments.[28] On the contrary, the oxime or nitrile structures, likely derived from the quinoid unit of PAni by reconstruction of the polymer backbone, can only be detected at high carbonization temperatures (>673 K),[29] and the imine N associated with the quinoid unit might eventually transform into pyridinic nitrogen (N6). Following these inspiring works, we intended to i) develop a method to moderate the different nitrogen configurations in the polymer, ii) further examine the impact on the nitrogen speciation of the yielded carbons, and iii) extend the scope to other polymeric materials.

Herein, we report a facile strategy to synthesize a family of highly N-doped carbons with tunable nitrogen functionalities by intensifying ring-opening of cross-linked polymer precursors through controlled pre-oxidation in flowing air, followed by conventional carbonization in inert stream (**Figure 1**). More importantly, the developed method is also effective when extrapolated to a total of six types of (co)polymers synthesized from the respective monomers with different natures. The impacts of pre-oxidation treatment on the nitrogen speciation, composition, structure, and morphology of the finally yielded NCs were systematically studied by coupling a spectrum of characterization techniques. Finally, we demonstrated the superiority of the highly N-doped carbons with enriched pyridinic nitrogen speciation as a new class of advanced functional materials in lithium ion batteries (LIBs) and in diverse catalytic applications, including the selective oxidation of different aromatic hydrocarbons and benzylic alcohols.

2. Results and Discussion

Our approach for the synthesis of highly N-doped carbons comprises the controlled peroxidation of a polymer precursor and a subsequent pyrolysis step. To demonstrate the broad applicability of this strategy, a total of six different polymers including three polyaniline-based polymers, that is, PAni, polyaniline-polypyrrol copolymer (PAniPy), and polyaniline-phytic acid complex (PAniPA), two polypyrroles (PPy and PPy-s) derived from different synthetic methods, and an additional polydopamine polymer (PDA), was targeted. Controlled oxidation of the polymers was mainly studied at 393–673 K as further increasing the temperature to 723 K led to significant combustion and very low yield of the carbonized sample (Figure S1, Supporting Information), and thus was not discussed hereafter.

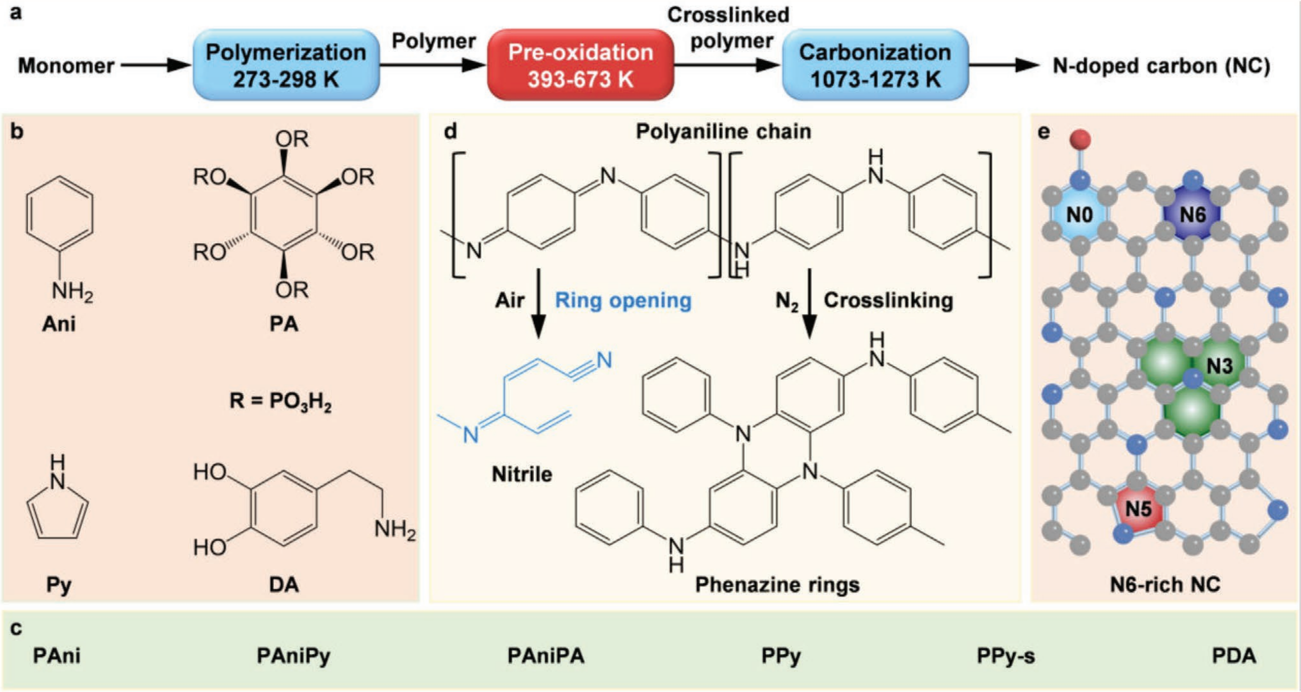

Figure 1. a) Synthetic strategy toward highly nitrogen-doped carbons e), comprising the polymerization of different monomers b), followed by controlled pre-oxidation, and carbonization of the corresponding polymers c). The pre-oxidation treatment has prominent influence on the development of different nitrogen functionalities of crosslinked polymers as exemplified with polyaniline d). Monomer: aniline (An), pyrrole (Py), phytic acid (PA), dopamine (DA). (Co)Polymers: polyaniline (PAni), polyaniline-polypyrrole (PAniPy), polyaniline-phytic acid (PAniPA), polypyrroles (PPy, PPy-s), polydopamine (PDA). Nitrogen speciation in NC: N6: pyridinic N, N5: pyrrolic N, N3: quaternary N, N0: oxidized pyridinic N.

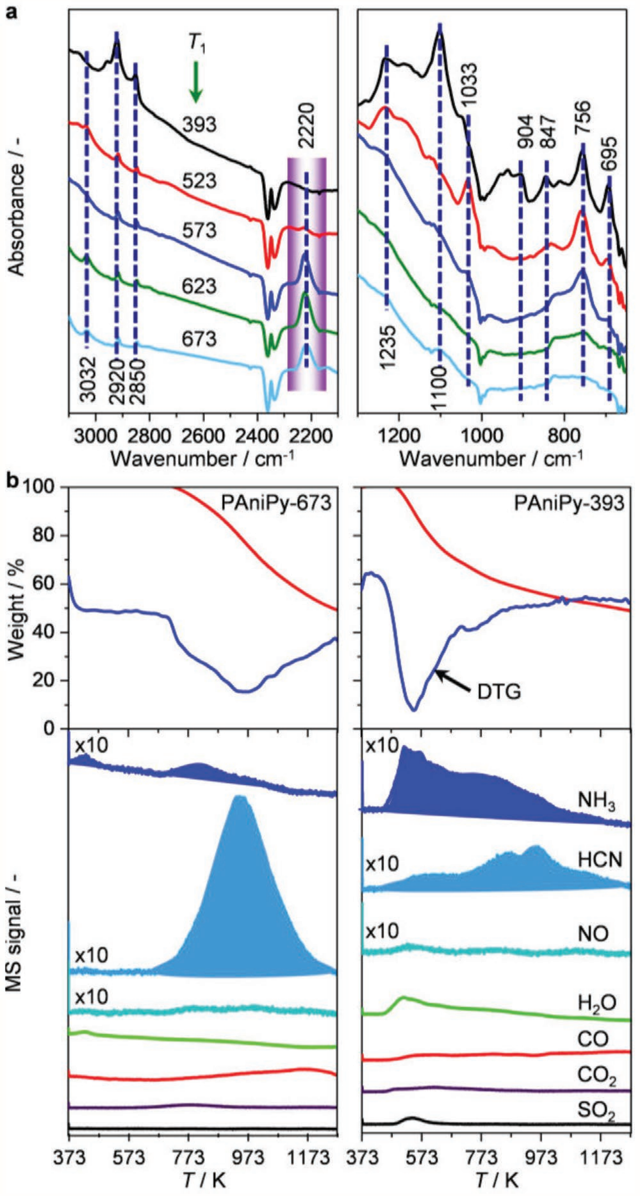

Figure 2. a) Ex situ DRIFT spectra of PAniPy polymers after pre-oxidizing at different temperatures (T_1), and b) the representative TG/DTG profiles in Ar accompanied with corresponding MS signals of various fragments.

2.1. Moderation of Nitrogen Functionalities of Polymer Precursors

First, diffuse reflectance infrared fourier transform spectroscopy (DRIFT) was employed to examine the variation of different functionalities of the polymers upon oxidation treatment. As a representative, **Figure 2**a shows the spectra of the PAniPy-T_1 (T_1 = pre-oxidation temperature in K) series. With the increasing oxidation temperature, most of the bands showed weakened intensities, including the C−H vibrations at 904, 1100, 2850, and 2920 cm^{-1}, two aniline oligomer-related vibrations at 695 and 756 cm^{-1}, and that of HSO_4^-/SO_3^- on sulfonated aromatic ring at 1033 cm^{-1}. In addition, the band at 1235 cm^{-1} that can be ascribed to ν(C−N) in the N,N′-diphenyl-1,4-phenylenediamine unit almost completely vanished at 573 K. Meanwhile, a new band at 2220 cm^{-1}, which was tentatively assigned to the nitrile (C≡N) or oxime (N=C=O) vibrations,[30,31] was already found at 523 K and the intensity increased with the pre-oxidation temperature. In stark contrast, this band showed much lower intensity in the polymer even after treated at 673 K in N_2 (Figure S2, Supporting Information). Another two polymers (PAni and PPy-s) subject to treatment in the different atmospheres were then checked, and similar observations were also found in both series despite the very different compositions (Figure S2, Supporting Information). These results suggested that, in comparison to the conventional direct carbonization wherein crosslinking of polymer chains is dominant in low temperature (<673 K),[28,30] the controlled oxidation treatment is a more disruptive manner even under milder conditions and thus promotes the formation of nitrile or oxime structures through ring opening in the polymers.

To gain more insight on the variations of different functionalities upon pre-treatment, the evolution of volatile species on the PAniPy-T_1 series was followed by thermogravimetric analysis (TGA) coupled with mass spectroscopy (TGA-MS, Figure 2b and Figure S3, Supporting Information). The PAniPy-393 showed a weight loss of ≈50 wt% upon 1273 K in Ar, accompanied with two distinct slopes: the low-temperature region at around 523 K is mainly associated with the release of NH_3 with relatively small contributions of HCN, H_2O, and SO_2, and the high-temperature region around 973 K is due to the development of both HCN and NH_3. The release of CO_x and NO was very weak in Ar, which was different from the case when running in O_2. The PAniPy-673 was then checked and its TG curve showed a similar weight loss of ≈50 wt% up to 1273 K, but with only one slope at the high-temperature around 973 K. The disappearance of the low-temperature weight loss suggests that pre-oxidation treatment at 673 K should be sufficient to partially release NH_3. In comparison to the PAniPy-393, this pre-treated sample shows prominent differences in the respective MS fragments. At first, the NH_3 signal became much weaker in PAniPy-673, whereas the HCN release was significantly promoted. Second, more CO was evolved and the peak was shifted to the high-temperature region. To verify whether such features are only associated with the copolymer, the PAni-T_1 series was also examined. Indeed, similar trends were observed on PAni-673, showing significantly enhanced releases of HCN and CO, and dramatically decreased amounts of NH_3 and CO_2 (Figure S4, Supporting Information). To better depict the evolution of different nitrogen speciation, the relative contribution of HCN and NH_3 was estimated by comparing the S_{HCN}:S_{NH_3} values of the polymers oxidized at 393 and 673 K, where S is the integration of respective fragment in the MS. For the PAniPy-T_1 series, these values are 0.8 (393 K) and 22.9 (673 K), and for the PAni-T_1 series, 0.4 (393 K) and 8.0 (673 K). The above findings clearly demonstrate that controlled oxidation is effective in moderating the relative contribution of different nitrogen functionalities of the polymers. By combining the DRIFT and TGA-MS results, it is further confirmed that the enhanced evolutions of HCN and CO, which are quite overlapping, might originate from the nitrile or oxime ensembles.

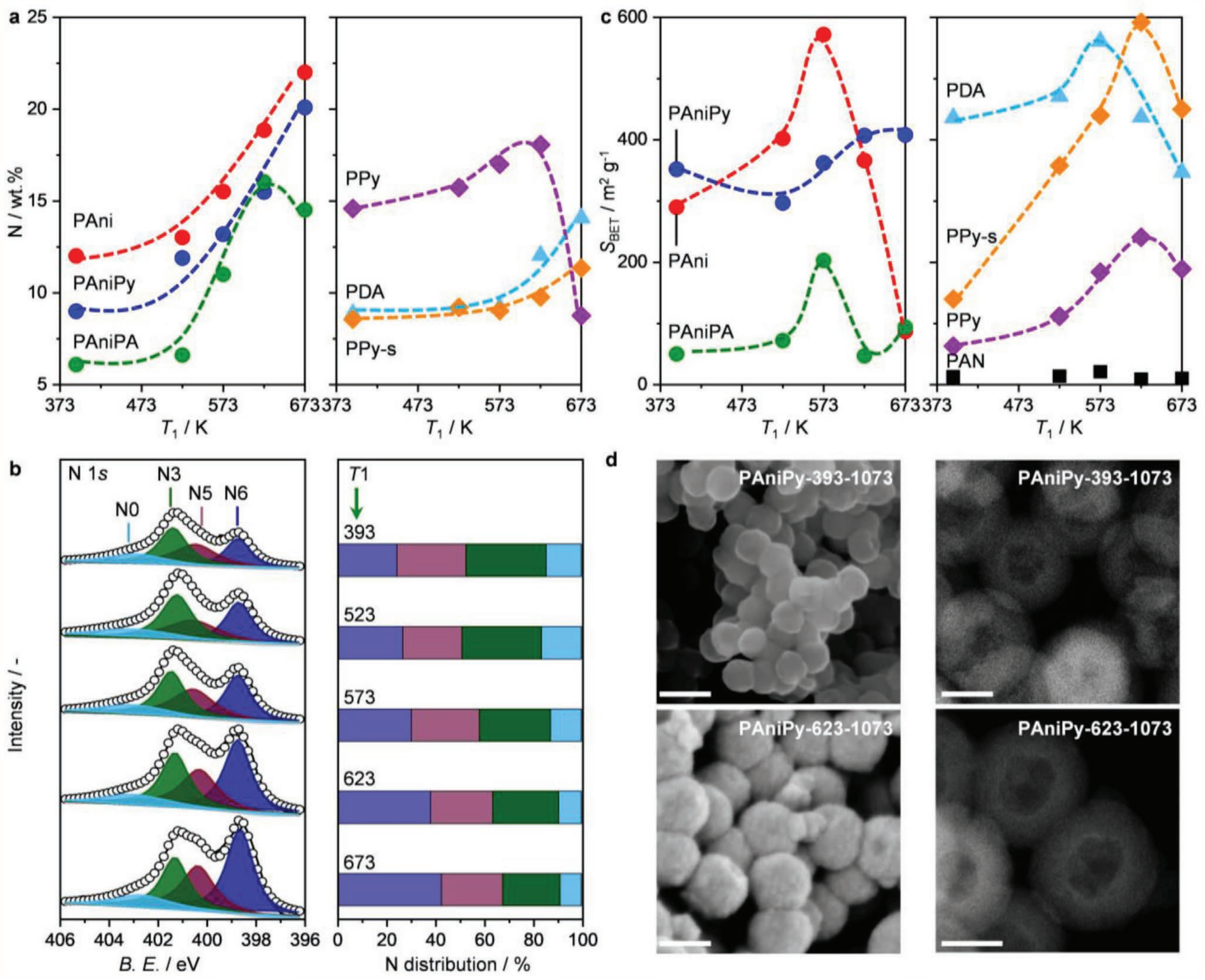

Figure 3. Characterization of N-doped carbons derived from different polymer precursors. a) The total nitrogen content, determined by the elemental analysis and b) the specific surface area (S_{BET}), determined by N_2 sorption, as a function of the pre-oxidation temperature for polyaniline-based and the rest (co)polymers. c) The deconvoluted N 1s XPS spectra of N-doped carbons derived from the PAniPy-T_1 series, accompanied with the distribution of different nitrogen speciation. d) HAADF-STEM images of selected N-doped carbons derived from the PAniPy polymers. Scale bars: 100 nm.

2.2. Speciation of Nitrogen-Doped Carbons

The polymers after pre-treatment at different temperatures were further converted to NC by carbonization in Ar at 1073 K. The C, N, and H contents of the polymers and the corresponding NCs were determined by elemental analysis (**Figure 3**a). Interestingly, the total nitrogen content can be increased to different extents with the pre-oxidation treatment, irrespective of the different polymers. The developed approach is most effective to the polyaniline-based polymers, that is, PAni, PAniPy, and PAniPA, for which the nitrogen content can be increased by 2–3 times, whereas the changes are relatively milder for the rest three polymers (<1.6 times). In addition, the maximal nitrogen content strongly depends on the pre-oxidation temperature. For most of the polymers it appeared at 673 K but shifted to 623 K for the PAniPA and PPy. Thus, the compositional and structural differences highlight the need for individual optimization of this parameter for different polymers. The dependence of the nitrogen content as a function of the carbonization temperature (1073–1273 K) was then examined on the PAni-T_1 series (Figure S5, Supporting Information). With elevated temperatures, however, the nitrogen content showed significant loss and the pre-oxidation effect became less prominent, probably because of the intrinsic instability of the nitrogen functionalities under such harsh pyrolysis conditions.

X-ray spectroscopy (XPS) was then performed to study the variations of different nitrogen speciation in NC after different pre-treatments. First, we compared the N 1s XPS spectra of the corresponding NCs derived for the PAniPy, PAni, and PPy with pre-oxidation at 393 and 673 K (Figure S6, Supporting Information). Typical two adjacent peaks at 396–404 eV binding energy (BE) can be found for all the samples, and in general, the contribution of the peak at low BE increased for all the samples pre-oxidized at higher temperatures, hinting similar trends in nitrogen speciation variation. To further elucidate this point, deconvolution was conducted for the whole PAniPy-T_1-1073 series (Figure 3b and Table S1, Supporting Information). In line with the earlier studies,[26] the presence of all the four kinds of nitrogen speciation was confirmed in all those samples, with N6, N5, and N3 as the major constitutes. With increasing the pre-treatment temperature, N6 steadily developed and the share reached from 24.0 to 42.3% while N3 showed an opposing trend, with the share decreased from 33.1 to 23.7%, as well as the N0. Besides, the share of N5 stayed relatively stable and did not show any clear dependence on the temperature variable.

The significant alterations in the total nitrogen content and the distribution of different speciation could be linked to the variations of nitrogen functionalities induced by the pre-oxidation treatment. TGA-MS analysis revealed that, instead of NH_3, HCN was the main N-containing species evolved during carbonization of the polymers pre-treated at 673 K, plus the release of a larger amount of CO_x. This would therefore lead to more carbon removed from the framework and a higher N:C ratio of the resulting NCs. On the other hand, the increased share of N6 speciation might be probably related to the favorable formation of nitrile and/or oxime ensembles as supported by both DRIFT and TGA-MS. In fact, these architectures are the derivatives of imines that have been proposed as the precursors to N6 speciation.[28,29]

2.3. Structural and Morphological Evolution

The structural variations, induced by the pre-treatment, of the N-doped carbons from different polymers were studied by N_2 sorption. The total surface area of the corresponding NCs as a function of T_1 is presented in Figure 3c. Volcano-like curves are observed for most of the samples with the maximal reached at 573–623 K, suggesting that mild oxidation of the polymers is most effective in the development of surface area and porosity, particularly the mesopores. The NCs from PAniPy are the only exception, for which the influence is marginal likely due to the special hollow nanosphere morphology (*vide infra*). The morphologies of selected NCs derived from the two polyaniline-based polymers were examined by scanning electron microscopy (SEM, Figure S7, Supporting Information), and showed a clear "memory effect." The PAni-T_1-1073 and PAniPA-T_1-1073 series both showed a similar inter-connected granular morphology like the polymer precursors, while the PAniPy-T_1-1073 series presented an interconnected nanosphere morphology. The unique morphology of PAniPy-T_1-1073 is a result of the simultaneous self-assembly of both aniline and pyrrole monomers around tergitol (surfactant), as has been discussed in an earlier study.[32] High-angle annular dark field scanning transmission electron microscopy (HAADF-STEM) analysis of this series further reveals that, different from the polymer precursor, the pyrolyzed samples display hollow morphology (Figure 3d and Figure S8, Supporting Information), which could be explained by the different thermal expansion coefficients of the two polymers. Furthermore, PAniPy-623 showed relatively larger inner and outer diameters than PAniPy-393, hinting that high-temperature pre-treatment is favorable for the development of hollow structures.

2.4. Applications of Highly Doped Carbons with Rich Pyridinic Nitrogen

As a class of abundant and relatively cheap materials, nitrogen-doped carbons have been extensively explored in broad fields such as adsorbent, battery, supercapacitor, and catalysis. Despite the great versatility in diverse applications, the studies exploring the potential of highly doped carbons, especially when coupled with systematic alternation in specific nitrogen speciation, are scarcely reported. In this context, the materials developed in our work can provide a great chance for this task. Accordingly, the performances of the whole PAniPy-T_1-1073 series as anode for lithium ion batteries and in the selective oxidation of aromatic hydrocarbons and benzylic alcohols were investigated. The PAniPy materials other than PAni and PAniPA was selected for applications based on two considerations: i) a wide range of nitrogen content (9–20 wt%) should be covered, and ii) the similar morphology and porosity (Table S2, Supporting Information) to exclude their impacts on Li ions storage and catalysis.

2.4.1. Electrochemical Performance for LIBs

We first tested the electrochemical performance of PAniPy-673-1073 in the voltage range of 0.01–3.0 V versus Li^+/Li. In the first discharge cycle (Figure S9a, Supporting Information), the typical cathodic peaks at 0.5–1.0 V were observed for PAniPy-673-1073, which was attributed to the formation of solid electrolyte interphase.[33] While the discharge peak at 1.66 V was likely caused by the irreversible reactions between Li ions and graphitic nitrogen in PAniPy-673-1073.[34] With the continuous cycling, the cathodic peaks disappeared, indicative of outstanding reversibility of PAniPy-673-1073 as anode for LIBs. Such phenomenon could also be observed from the change of the discharge plateau in galvanostatic charge-discharge (GCD) profiles (Figure S9b, Supporting Information). With increasing the pre-oxidation temperature from 393 to 673 K, the capacities of PAniPy-T_1-1073 materials were gradually enhanced from 451 mAh g^{-1} for PAniPy-393-1073, 493 mAh g^{-1} for PAniPy-523-1073, 549 mAh g^{-1} for PAniPy-573-1073, 690 mAh g^{-1} for PAniPy-623-1073 to the highest value of 879 mAh g^{-1} for PAniPy-673-1073 (**Figure 4**a). The progressive improvement of the capacity was largely ascribed to the gradual increase of N-doped content in the PAniPy-T_1-1073 series, especially for the pyridinic nitrogen with stronger adsorption ability of Li ion. Most importantly, PAniPy-673-1073 via pre-oxidation and carbonization process showed a higher capacity than most of the state-of-the-art N-doped carbon-based anodes for LIBs (Table S3, Supporting Information), for instance, N-doped porous graphene (742 mAh g^{-1}),[35] N-doped graphene sheets (832.4 mAh g^{-1}),[34] N-doped carbon spheres (666 mAh g^{-1}),[36] demonstrating that the developed pre-oxidation and carbonization polymer method is a feasible strategy to introduce more electronegative N-heteroatom with high doping level in carbon-based materials, catering for notably improved electrochemical performance for Li ion storage. Furthermore, albeit possessing the lowest specific surface area (87 m^2 g^{-1}) in PAni-T-1073 anodes, the PAni-673-1073 exhibited the most abundant

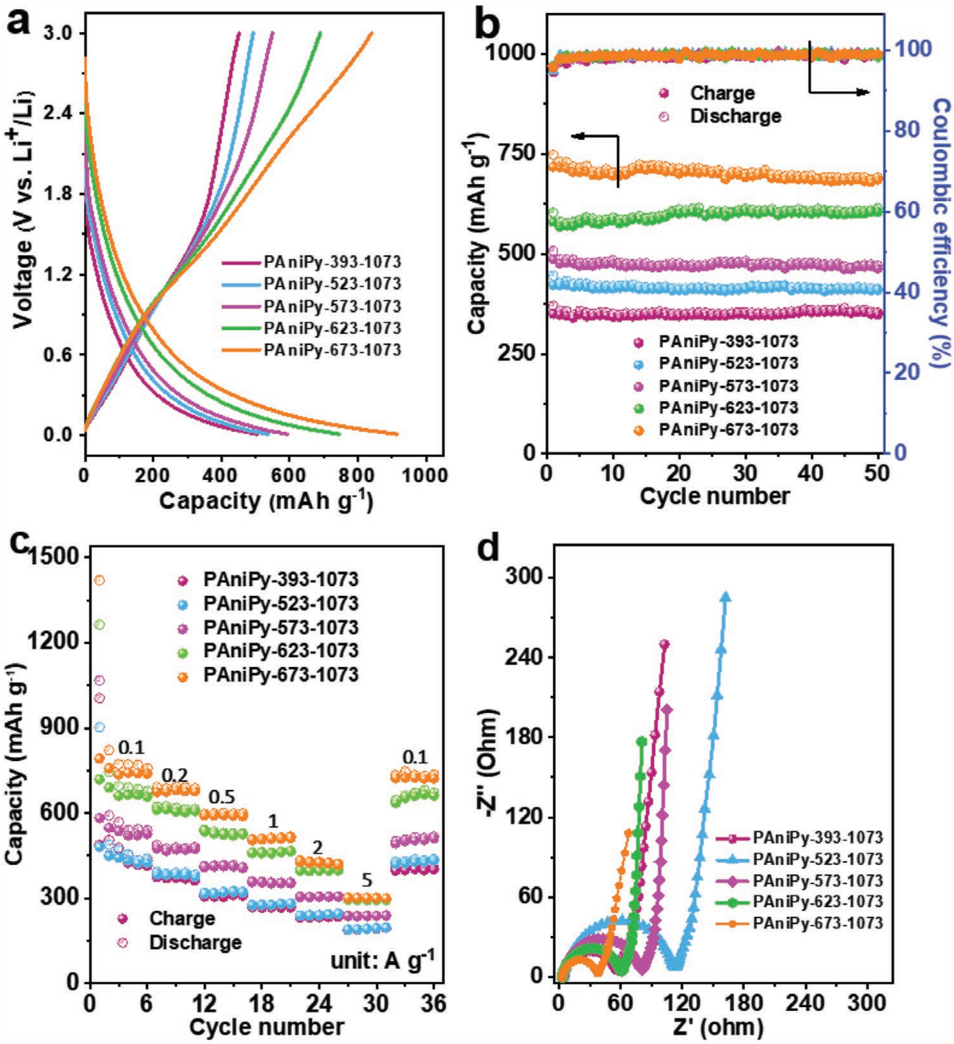

Figure 4. Electrochemical performance of PAniPy-T_1-1073 as anode for LIBs in $LiPF_6$ electrolyte in the potential of 0.01 to 3.0 V versus Li^+/Li. a) GCD profiles measured at 0.1 A g^{-1}. b) Cycling performance tested at 0.2 A g^{-1}. c) Rate capability recorded at different current densities from 0.1 to 5 A g^{-1}. d) EIS profiles.

nitrogen content (22.0%) and delivered the highest capacity of 634 mAh g^{-1} at 0.1 A g^{-1} (Figure S9, Supporting Information), much higher than PAni-393-1073 (508 mAh g^{-1}), PAni-523-1073 (574 mAh g^{-1}), PAni-573-1073 (582 mAh g^{-1}), and PAni-623-1073 (527 mAh g^{-1}). It strongly suggests that the high nitrogen level plays a more important role in improving capacity other than large specific surface area. However, the capacity of PAni-673-1073 (634 mAh g^{-1}) was still inferior to that of PAniPy-673-1073 (879 mAh g^{-1}), due to the agglomerate bulks of PAni under higher pre-oxidation temperature. In addition, the PAniPy-673-1073 electrode showed reversible capacity of 685 mAh g^{-1} at 0.2 A g^{-1} in the 50th cycle (Figure 4b), which is approximately two times higher than that of PAniPy-393-1073 (348.3 mAh g^{-1}), strongly suggestive of robust lithium storage performance of PAniPy-673-1073 in term of high capacity and long lifespan. Remarkably, the PAniPy-673-1073 still exhibited satisfactory capacity of 301 mAh g^{-1} even at a high current density of 5 A g^{-1} (Figure 4c and Figure S10c, Supporting Information), and a reversible capacity of PAniPy-673-1073 with ≈725 mAh g^{-1} was regained when the current density was suddenly switched to 0.1 A g^{-1}. The excellent rate capability of PAniPy-673-1073 is strongly related to the fast charge transfer process, proved by the electrochemical impedance spectra (EIS) of PAniPy-673-1073 with lower semicircle (R_{ct} = 34.6 Ω) in the high frequency region (Figure 4d). Furthermore, the long-term cycle life of PAniPy-673-1073 was demonstrated for 400 continuous charge-discharge cycles at 2 A g^{-1} with a tiny average capacity loss of only 0.078% per cycle, and an outstanding CE of more than 99.8% (Figure S10d, Supporting Information).

2.4.2. Selective Oxidations

Distinct features can be observed over the PAniPy-T_1-1073 series in the selective oxidation of benzyl alcohol (**Figure 5**a). First, the conversion level showed a volcano-like curve dependence on the pre-treatment temperature, and at 623 K it reached the maximal that is twofold higher than that of conventional

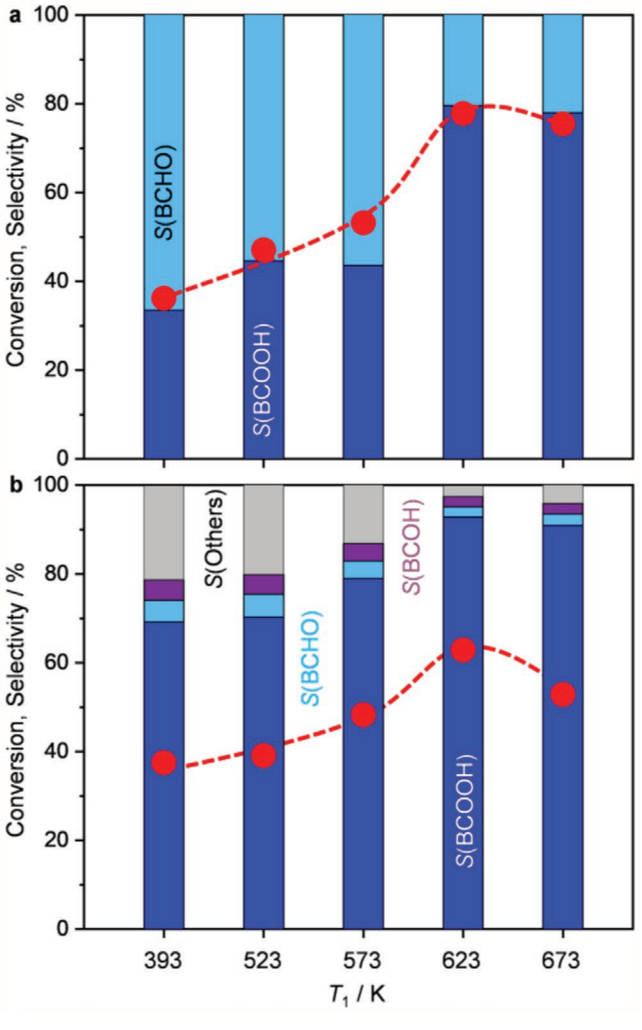

Figure 5. Catalytic performance of PAniPy-T_1-1073 in the selective oxidation of a) benzyl alcohol (BCOH) and b) toluene. Reaction conditions: substrate, 1 mmol, H_2O, 3 cm^3, TBHP (70 wt% in H_2O), 0.5 cm^3, catalyst, 10 mg, $T = 373$ K, and $t = 6$ h. Conversion and selectivity are indicated by the circles and bars, respectively. BCHO, benzaldehyde; benzoic acid, BCOOH.

PAniPy-393-1073. Second, the selectivity of benzoic acid, the deep oxidation product, increased steadily (from 33 to 80%) at the compensation of benzaldehyde with the rising pre-treatment temperature. Replacing air with O_2 gives excellent yield of benzoic acid (99%) over the best-performed PAniPy-623-1073, which is remarkable among the metal-free carbon-based catalysts (Table S4, Supporting Information). When evaluated in toluene oxidation (Figure 5b), a similar activity trend was observed as in the oxidation of benzyl alcohol, with the maximal of 1.7-fold increase in conversion level for PAniPy-623-1073. Besides, the selectivity of benzoic acid, the major product over the whole series, also increased (from 69 to 93%), and more importantly the side-reactions were largely prohibited (total byproduct selectivity decreased from 21 to 2%). To verify if the above phenomenon was only associated with the specific substrates, two additional substrates (cinnamyl alcohol and ethylbenzene) were also studied (Figure S11, Supporting Information). Like in the toluene oxidation, PAniPy-623-1073 showed more than twofold increase in activity (from 36 to 74%) and acetophenone selectivity (from 37 to 87%), with significantly reduced byproduct selectivity (from to 51% to 0.6%). For cinnamyl alcohol, a more challenging substrate, PAniPy-673-1073 was the best-performing catalyst, showing 1.3-fold activity increase in comparison to PAniPy-393-1073. Notably, it can also promote the formation of cinnamic acid that is not detected on PAniPy-393-1073. These results demonstrated that the highly nitrogen-doped carbons can not only significantly boost the catalytic activity but also moderate the reaction path and product distribution, thus might open up more possibilities in other applications.

2.4.3. Structure-Performance Relationships

To shed light on the distinct behaviors of the highly N-doped carbon, tentative correlations between the electrochemical and catalytic activity and the total and respective nitrogen speciation were made in order to establish the structure-performance relationships (**Figure 6**). Since the share of N3 species stayed relatively stable in this series while the N0 sites are in minor percentage on the basis of XPS, these speciations were not further considered. Interestingly, the capacity in LIBs increased almost linearly with the total nitrogen as well as the share of N6 sites. As compared with carbon atoms, the high doping content of nitrogen with higher electronegativity is much beneficial to the formation of a robust bonding to Li ions, leading to the remarkable enhancement of capacity with the N content increased. Furthermore, the defects created by the heteroatoms, especially for the pyridinic-N and pyrrolic-N,[35] are able to serve as a significant role in accommodating or adsorbing Li ions, further contributing to the improvement of Li ion storage. In catalysis, the correlations of benzoic acid yield as a function of the total nitrogen, and the shares of N6 and N3 sites showed volcano-like dependency. The promotional effect of high nitrogen content is evidenced from the significantly boosted activity, particularly at 9–16 wt%, albeit the activity slightly dropped at even higher nitrogen content. The latter suggested that the individual nitrogen speciation should also play a role in determining the performance. Indeed, the activity developed almost linearly with the increasing share of N6 species in a very wide range (22–37 at%), strongly hinting its decisive contribution in the catalytic cycles. Further increasing the N6 share led to loss of activity, which might be caused by the sacrificing of the N3 functionalities.

3. Conclusion

In this work, we have developed a general strategy to fabricate a new family of highly doped carbon materials (up to 22 wt% N) with tunable nitrogen speciation, and demonstrated the great versatility for a wide range of different (co)polymers. Combining controlled pre-oxidation treatment with conventional carbonization led to a two- to threefold increase in total nitrogen content and the favored development of pyridinic N at the expense of quaternary N species. These can be rationalized by

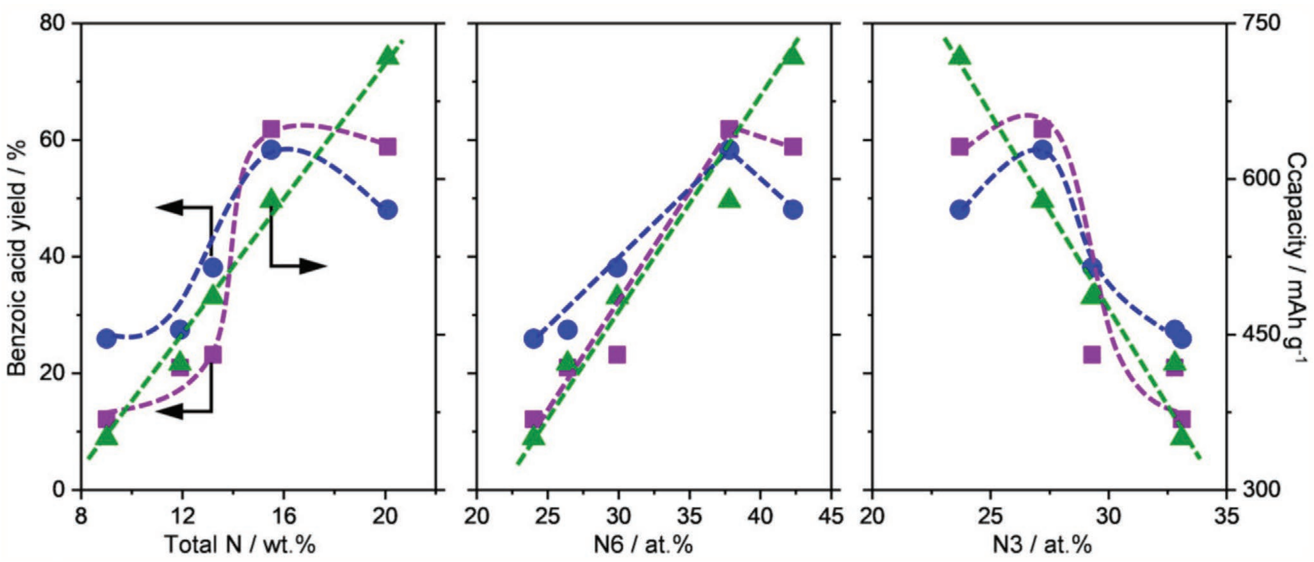

Figure 6. Correlations of the catalytic and electrochemical performances of the PAniPy-T_1-1073 series as a function of the total nitrogen and the shares of N6 and N3 speciation. The yield of benzoic acid was used as the activity descriptor in benzyl alcohol (squares) and toluene (circles) oxidation, while the capacity of charge at the first cycle tested at 0.2 A g^{-1} was taken. The dashed lines are for purpose of eye guide.

the alternation of nitrogen functionalities upon oxidation of the polymers, as multiple characterization techniques revealed the favorable formation of nitrile or oxime ensembles, hinting the intensified ring-opening of cross-linked polymers under oxidative ambience. Furthermore, these novel functional materials show distinct behaviors in electrochemical cell and catalysis, differing markedly from those of conventional N-doped carbons. The developed highly doped pyridinic nitrogen-rich carbons show a remarkable capacity of 879 mAh g^{-1} at 0.2 A g^{-1} and excellent cycling performance in LIBs, and significantly boosted activity and altered product distribution in the selective oxidation of diverse aromatic hydrocarbons and benzylic alcohols. Finally, given the great versatility of our synthetic strategy and the broad applications of metal-free carbon materials, we anticipate that our study will also have implications for future studies in other catalysis, batteries, and supercapacitors, wherein the tunable nitrogen speciation of these materials provides an excellent chance to establish the material design rules.

4. Experimental Section

Material Synthesis: The polyaniline-polypyrrol copolymer (denoted as PAniPy) was synthesized following a previously established protocol[28] with a few modifications. A mixture of tergitol (92.4 mg, Sigma-Aldrich, type 15-S-9), aniline (50 mmol, Acros, 99.5%), and pyrrole (50 mmol, Sigma-Aldrich, 98%) was dissolved in 160 cm^3 deionized water, and stirred at 500 rpm in an ice bath for 30 min. Another solution of ammonium persulfate (4.56 g, Acros Organics, 98%, dissolved in 40 cm^3 deionized water) was prepared, cooled at ice bath for 30 min, and added dropwise into the above solution under vigorous stirring. Afterward, stirring was continued in the ice bath for another 1 h, and the polymerization was continued for another 23 h at room temperature. The yielded solid was filtrated, washed with deionized water, and dried at 373 K overnight.

The synthesis of polyaniline (PAni),[26] polypyrrole (PPy),[6] polydopamine (PDA),[37] and the polyaniline-phytic acid complex (PAniPA)[38] was conducted following the respective procedures reported in the earlier literature, and was detailed in the Supporting Information. An additional type of polypyrrole (PPy-s) was also prepared following the synthetic protocol of PAniPy but in the absence of aniline.

The as-prepared polymers were further converted to corresponding N-doped carbons in a tubular oven by the following two steps: first pre-oxidized in flowing air at different temperatures (T_1, 393, 523, 573, 623, 673 K, 2 K min^{-1}, 3 h), and then further carbonized in following N_2 at a higher temperature (1073 K, if not otherwise specified).

Characterization Methods: Elemental analysis of C, H, N, and O was determined by infrared spectroscopy using a LECO TruSpec Micro and a LECO 628 O Micro combustion furnace, respectively. Nitrogen adsorption and desorption isotherms were recorded using a Micromeritics TriStar analyzer instrument. Prior to analysis, samples were degassed overnight at 393 K. Diffuse reflectance infrared Fourier transform spectroscopy (DRIFTS) were recorded on a Bruker Vertex 400 spectrometer equipped with liquid N_2 cooled MCT detector and a Harrick diffuse reflection accessory (4000–700 cm^{-1}, 4 cm^{-1} resolution, 32 scans). Prior to analysis, samples were degassed in Ar (20 cm^3 min^{-1}) for 1 h. TGA was performed in a Mettler Toledo TGA/DSC 1 Star system connected to a Pfeiffer Vacuum Thermo-Star GDS 320 T1 mass spectrometer (MS). The program involved dehydrating the samples at 373 K in flowing air followed by ramping the temperature from 373 to 1073 K at a rate of 10 K min^{-1} all under argon or flowing air (100 cm^3 min^{-1}). The fragments with m/e of 18, 28, and 44 were followed by MS indicative of H_2O, CO, and CO_2, respectively. X-ray photoelectron spectroscopy (XPS) was measured in a Physical Electronics Quantum 2000 X-ray photoelectron spectrometer using monochromatic Al-Ka radiation, generated from an electron beam operated at 15 kV, and equipped with a hemispherical capacitor electron-energy analyzer. The solids were analyzed at the electron take-off angle of 45° and the pass energy of 46.95 eV. The spectrometer was calibrated for the Au $4f_{7/2}$ signal to be at 84.0 ± 0.1 eV and had a resolution step width of 0.2 eV. The N 1s envelopes were fitted by mixed Gaussian–Lorentzian component profiles after Shirley background subtraction. The selected peak positions of the different nitrogen species were based on literature reported data and fixed with an error of ±0.2 eV. The elemental concentrations were quantified based on the measured photoelectron peak areas (C 1s and N 1s) after Shirley background subtraction, using PHI-MultiPak software and the built-in relative sensitivity factors, which were corrected for the system transmission function. SEM was conducted on a Quanta 200F instrument operating at 10 kV and 50 pA. The powder sample was dispersed in dry form onto fresh carbon paint deposited on an aluminum holder and subsequently coated by a Pt-Pd alloy (≈10 nm thickness) to prevent charging. STEM micrographs with a HAADF detector were acquired on a Talos F200X instrument (Thermos Fisher Scientific) operated at 200 kV.

Electrochemical Tests: Lithium ion batteries were assembled at CR2016 coin cells using lithium foil as the counter and reference electrode, PAniPy-*T*-1073 electrode as working electrode, and commercial LB-113 as electrolyte. The working electrodes were prepared through the mixture of N-doped carbon powder, carbon black, and polyvinylidene fluoride with a weight ratio of 8:1:1 in N-methylpyrrolidone solvent. The resultant electrode slurry was pasted onto a copper current collector, followed by vacuum drying at 393 K for 12 h, and then cut into electrode plate with a diameter of 12 mm. The GCD profiles were operated at a LAND CT2001A battery tester in a voltage range from 0.01 to 3.0 V. EIS and cyclic voltammetry (CV) curves were carried out at a CHI 760E workstation. The CV tests were conducted at 0.01–3.0 V with a scanning rate of 0.1 mV s^{-1}. The EIS data were collected at an ac amplitude of 5 mV with the frequency range from 100 to 0.1 Hz.

Catalytic Tests: The selective oxidation of two benzylic alcohols (benzyl alcohol, 99.8%, Sigma-Aldrich, cinnamyl alcohol, Sigma-Aldrich, 98%) and two aromatic hydrocarbons (toluene, TCI, 99.5%, ethylbenzene, Acros Organics, 99.8%) was studied in pressure tube reactors (V = 21 cm^3, Ace Glass) equipped with a magnetic stirrer and heated using an oil bath. In a typical experiment, the pre-dried catalyst (10 mg, 373 K, 12 h), and a solution of the substrate (1 mmol) in deionized water (3 cm^3) and tert-butyl hydroperoxide (TBHP, 3 cm^3, Sigma-Aldrich, 70 wt% in H_2O) were added to the reactor. After replacing air with Ar three times, the reactor was sealed and heated to 373 K at autogenous pressure for 6 h. The reaction mixture was quenched with ice-water. After separation of the solid by centrifugation, the organics were extracted with cyclohexane (3 cm^3, ABCR, 99%) and 0.01 cm^3 of the oil phase was added to 1 cm^3 acetonitrile (AcroSeal, 99.9%) for further analysis. Samples were analyzed using an Agilent 1260 Infinity HPLC equipped with an Agilent Zorbax C18 column (150 × 3.0 mm, 3 μm, 298 K) and both DAD and RID detectors. The substrate and product concentrations were calibrated with reference to pure standards.

Supporting Information

Supporting Information is available from the Wiley Online Library or from the author.

Acknowledgements

X.M., J.M., and S.Z. contributed equally to this work. This work was financially supported by the National Key R&D Program of China (Grants 2016YBF0100100, 2016YFA0200200), National Natural Science Foundation of China (Grants 51872283, 21805273), Liaoning BaiQianWan Talents Program, Natural Science Foundation of Liaoning Province, Joint Research Fund Liaoning-Shenyang National Laboratory for Materials Science (Grant 20180510038), Liaoning Revitalization Talents Program (Grant XLYC1807153), DICP (DICP ZZBS201708, DICP ZZBS201802, DICP I202032), DNL Cooperation Fund, CAS (DNL180310, DNL180308, DNL201912, and DNL201915), DICP&QIBEBT (Grant DICP&QIBEBT UN201702). The authors thank Dr. A. Martin and Dr. J. Zhang for the assistance with SEM. ScopeM of ETH Zurich is acknowledged for the use of their facilities.

Conflict of Interest

The authors declare no conflict of interest.

Keywords

catalysis, lithium ion battery, nitrogen-doped carbon, polymers, synthetic strategy

Received: July 18, 2020
Revised: September 15, 2020

---

[1] X. Liu, L. Dai, *Nat. Rev. Mater.* **2016**, *1*, 16064.
[2] L. He, F. Weniger, H. Neumann, M. Beller, *Angew. Chem., Int. Ed.* **2016**, *55*, 12582.
[3] X.-K. Kong, C.-L. Chen, Q.-W. Chen, *Chem. Soc. Rev.* **2014**, *43*, 2841.
[4] J. W. F. To, J. J. He, J. G. Mei, R. Haghpanah, Z. Chen, T. Kurosawa, S. C. Chen, W. G. Bae, L. J. Pan, J. B. H. Tok, J. Wilcox, Z. N. Bao, *J. Am. Chem. Soc.* **2016**, *138*, 1001.
[5] J. J. He, J. W. F. To, P. C. Psarras, H. P. Yan, T. Atkinson, R. T. Holmes, D. Nordlund, Z. N. Bao, J. Wilcox, *Adv. Energy Mater.* **2016**, *6*, 1502491.
[6] M. Sevilla, P. Valle-Vigón, A. B. Fuertes, *Adv. Funct. Mater.* **2011**, *21*, 2781.
[7] W. Guo, X. Li, J. Xu, H. K. Liu, J. Ma, S. X. Dou, *Electrochim. Acta* **2016**, *188*, 414.
[8] X. Li, J. Liu, Y. Zhang, Y. Li, H. Liu, X. Meng, J. Yang, D. Geng, D. Wang, R. Li, *J. Power Sources* **2012**, *197*, 238.
[9] Y. Xie, Y. Chen, L. Liu, P. Tao, M. Fan, N. Xu, X. Shen, C. Yan, *Adv. Mater.* **2017**, *29*, 1702268.
[10] N. Daems, X. Sheng, I. F. Vankelecom, P. P. Pescarmona, *J. Mater. Chem. A* **2014**, *2*, 4085.
[11] C. Hu, L. Dai, *Angew. Chem., Int. Ed.* **2016**, *55*, 11736.
[12] H. B. Yang, J. Miao, S.-F. Hung, J. Chen, H. B. Tao, X. Wang, L. Zhang, R. Chen, J. Gao, H. M. Chen, *Sci. Adv.* **2016**, *2*, e1501122.
[13] K. Chizari, A. Deneuve, O. Ersen, I. Florea, Y. Liu, D. Edouard, I. Janowska, D. Begin, C. Pham-Huu, *ChemSusChem* **2012**, *5*, 102.
[14] W. Qi, D. Su, *ACS Catal.* **2014**, *4*, 3212.
[15] D. S. Su, J. Zhang, B. Frank, A. Thomas, X. Wang, J. Paraknowitsch, R. Schlögl, *ChemSusChem* **2010**, *3*, 169.
[16] W. Ding, Z. Wei, S. Chen, X. Qi, T. Yang, J. Hu, D. Wang, L. J. Wan, S. F. Alvi, L. Li, *Angew. Chem., Int. Ed.* **2013**, *52*, 11755.
[17] B. He, F. Liu, S. Yan, *J. Mater. Chem. A* **2017**, *5*, 18064.
[18] M. S. Lee, H.-J. Choi, J.-B. Baek, D. W. Chang, *Appl. Energy* **2017**, *195*, 1071.
[19] Z. Luo, S. Lim, Z. Tian, J. Shang, L. Lai, B. MacDonald, C. Fu, Z. Shen, T. Yu, J. Lin, *J. Mater. Chem.* **2011**, *21*, 8038.
[20] H. Miao, S. Li, Z. Wang, S. Sun, M. Kuang, Z. Liu, J. Yuan, *Int. J. Hydrogen Energy* **2017**, *42*, 28298.
[21] J. Wu, L. Ma, R. M. Yadav, Y. Yang, X. Zhang, R. Vajtai, J. Lou, P. M. Ajayan, *ACS Appl. Mater. Interfaces* **2015**, *7*, 14763.
[22] Y. Xia, R. Mokaya, *Chem. Mater.* **2005**, *17*, 1553.
[23] L. Zhang, Z. Su, F. Jiang, L. Yang, J. Qian, Y. Zhou, W. Li, M. Hong, *Nanoscale* **2014**, *6*, 6590.
[24] T. Z. Yang, T. Qian, M. F. Wang, X. W. Shen, N. Xu, Z. Z. Sun, C. L. Yan, *Adv. Mater.* **2016**, *28*, 539.
[25] T. Z. Yang, M. F. Wang, J. Liu, J. Q. Zhou, Z. Z. Sun, M. Z. Chen, C. L. Yan, *J. Mater. Chem. A* **2015**, *3*, 6291.
[26] R. Lin, S. K. Kaiser, R. Hauert, J. Perez-Ramirez, *ACS Catal.* **2018**, *8*, 1114.
[27] M. Trchova, P. Matejka, J. Brodinova, A. Kalendova, J. Prokes, J. Stejskal, *Polym. Degrad. Stab.* **2006**, *91*, 114.
[28] S. Kuroki, Y. Hosaka, C. Yamauchi, *Carbon* **2013**, *55*, 160.
[29] M. Trchova, E. N. Konyushenko, J. Stejskal, J. Kovarova, G. Ciric-Marjanovic, *Polym. Degrad. Stab.* **2009**, *94*, 929.

[30] Z. Rozlivkova, M. Trchova, M. Exnerova, J. Stejskal, *Synth. Met.* **2011**, *161*, 1122.
[31] M. Trchová, J. Stejskal, *Pure Appl. Chem.* **2011**, *83*, 1803.
[32] C. Zhou, J. Han, G. Song, R. Guo, *J. Polym. Sci., Part A: Polym. Chem.* **2008**, *46*, 3563.
[33] X. Liu, J. Zhang, S. Guo, N. Pinna, *J. Mater. Chem. A* **2016**, *4*, 1423.
[34] L. L. Tian, X. Y. Wei, Q. C. Zhuang, C. H. Jiang, C. Wu, G. Y. Ma, X. Zhao, Z. M. Zong, S. G. Sun, *Nanoscale* **2014**, *6*, 6075.
[35] Z.-Y. Sui, C. Wang, Q.-S. Yang, K. Shu, Y.-W. Liu, B.-H. Han, G. G. Wallace, *J. Mater. Chem. A* **2015**, *3*, 18229.
[36] D. Li, L.-X. Ding, H. Chen, S. Wang, Z. Li, M. Zhu, H. Wang, *J. Mater. Chem. A* **2014**, *2*, 16617.
[37] K. Ai, Y. Liu, C. Ruan, L. Lu, G. Lu, *Adv. Mater.* **2013**, *25*, 998.
[38] J. W. F. To, Z. Chen, H. Yao, J. He, K. Kim, H.-H. Chou, L. Pan, J. Wilcox, Y. Cui, Z. Bao, *ACS Cent. Sci.* **2015**, *1*, 68.